TU Delft

Delft University of Technology

Simulation of shotnoise induced side-wall roughness in electron lithography

Verduin, T.; Lokhorst, S. R.; Hagen, C. W.; Kruit, P.

DOI
10.1117/12.2219295

Publication date
2016

Document Version
Final published version

Published in
Metrology, Inspection, and Process Control for Microlithography XXX

Citation (APA)
Verduin, T., Lokhorst, S. R., Hagen, C. W., & Kruit, P. (2016). Simulation of shotnoise induced side-wall roughness in electron lithography. In M. I. Sanchez, & V. A. Ukraintsev (Eds.), *Metrology, Inspection, and Process Control for Microlithography XXX* (Vol. 9778). Article 97781Z (Proceedings of SPIE; Vol. 9778). SPIE. https://doi.org/10.1117/12.2219295

Important note
To cite this publication, please use the final published version (if applicable).
Please check the document version above.

Copyright
Other than for strictly personal use, it is not permitted to download, forward or distribute the text or part of it, without the consent of the author(s) and/or copyright holder(s), unless the work is under an open content license such as Creative Commons.

Takedown policy
Please contact us and provide details if you believe this document breaches copyrights.
We will remove access to the work immediately and investigate your claim.

This work is downloaded from Delft University of Technology.
For technical reasons the number of authors shown on this cover page is limited to a maximum of 10.

Simulation of shotnoise induced side-wall roughness in electron lithography

T. Verduin,* S. R. Lokhorst, C. W. Hagen, and P. Kruit

Delft University of Technology
Faculty of Applied Sciences
Department of Imaging Physics
Lorentzweg 1, 2628 CJ Delft, The Netherlands

ABSTRACT

We have developed a fast three dimensional Monte-Carlo framework for the investigation of shotnoise induced side-wall roughness (SWR) formation. The calculation outline is demonstrated by an exposure of a 100 nm thick layer of chemically amplified resist (CAR) on top of an infinitely thick silicon substrate. We use our home built Monte-Carlo electron-matter interaction simulator for the purpose of lithography. A pattern of an isolated line is written into the resist layer by scanning a beam with 20 keV electrons over an area of 32 nm×1 μm (width and length). During the exposure, we use a spot size of 20 nm, beam step size of 4 nm and a Poisson distributed exposure dose of 80 μC/cm^2, 60 μC/cm^2 and 40 μC/cm^2. During the exposure of the sample, we record the locations of the inelastic events within the resist layer. The distribution of released acids is determined under the simplified assumption that every inelastic event corresponds to a release. We now construct a three dimensional image of the (in)solubility of the resist layer within a cuboid of 128 nm(256px) wide, 800 nm(1024px) in length and 100 nm(128px) in height. The (in)solubility is obtained by summing the contribution of all acids to every voxel in the three dimensional image, where we have used a three dimensional Gaussian with $\sigma_{x,y,z} = r_d$ =5 nm for the diffusion of the acid. The boundary between exposed and unexposed resist is determined by a threshold. The resulting image of the (in)solubility is analyzed in different ways by considering slices and three dimensional views of the boundary. The average line edge roughness (LER) is obtained by calculating the standard deviation of the left and right boundary from yz-slices. By considering all slices, ranging from the top of the resist layer to the bottom of the substrate, the average LER as a function of the depth from the top surface of the resist layer is obtained. Shotnoise effects are observed as we decrease the exposure dose. An increased effect of shotnoise is observed near the vacuum and substrate interface. One contribution relates to the actual number of acids, which due to the scattering is less near the interface than away from the interface. Another contribution stems from the fact that no acids are found on the vacuum side nor on the substrate side.

Keywords: Simulation, Monte Carlo methods, Dimensional metrology, Lithography, Shotnoise

*Electronic address: `T.Verduin@tudelft.nl`

Metrology, Inspection, and Process Control for Microlithography XXX, edited by Martha I. Sanchez, Vladimir A. Ukrainstev
Proc. of SPIE Vol. 9778, 97781Z · © 2016 SPIE · CCC code: 0277-786X/16/$18 · doi: 10.1117/12.2219295

Downloaded From: http://proceedings.spiedigitallibrary.org/ on 03/13/2017 Terms of Use: http://spiedigitallibrary.org/ss/termsofuse.aspx

1. INTRODUCTION

The throughput of a lithographic system is an important parameter in a typical production line. This parameter can be increased in several ways. In optical lithography, for example, a more powerful source is one solution. In electron-beam lithography, an increase of the number of parallel beams is another solution. In either case, the use of a more sensitive chemically amplified resist would result in a reduction of the required exposure dose, and hence a reduction of the exposure time. In order to maximize throughput, it is tempting to choose the most sensitive CAR with the lowest possible illumination dose. In that limit, however, an increase of LER, and hence an insufficient control of critical dimension (CD) is observed.[1] This increase of LER is primarily caused by fundamental quantum noise (shotnoise) effects and becomes the dominant mechanism in the formation of LER.[2–8] Our attempt, in this theoretical study, is to develop an extended Monte-Carlo framework for the investigation of shotnoise induced SWR formation in CARs. We extend the existing studies in two different ways: (1) by including the interaction of the electron beam with a CAR through an advanced Monte-Carlo electron-matter interaction simulator and (2) by considering a full three dimensional model which, in contrast to Refs. 4–6, includes near-surface effects of acid diffusion. We expect that this extended model provides more insight in the effects on SWR of changing parameters such as resist thickness, acid diffusion and dose distribution. We will explain the method of SWR formation within this framework and give a striking example with analysis to demonstrate its use.

2. METHOD OF SWR FORMATION

At first, a (thin) layer of CAR is defined on top of an infinitely thick substrate. We now use the simulator of Ref. 9 for lithography: the electron beam is scanned over the sample such that a particular pattern is written. During the exposure, we record where the inelastic events take place within the resist layer. Next, we determine the distribution of released acids from the inelastic events under the following three assumptions. We assume that the initial distribution of photo acid generators (PAGs) in the resist layer is homogeneous and isotropic. Furthermore, we assume that every inelastic event in the simulation is associated with the release of an acid from a PAG. We emphasize that, for realistic studies, the probability for the release of an acid as a function of the kinetic energy of the electron must be included. In addition, we assume that a secondary electron is created in the inelastic event. The distribution of acids is then used to determine the breaking/making of bonds in the resist by considering a diffusion like process in the post exposure baking (PEB) phase. The (in)solubility at position (x, y, z) in the resist layer is determined by substituting each acid with a three dimensional Gaussian distribution,

$$S(x,y,z) \sim \sum_{i=0}^{n_{\text{acid}}-1} \exp \frac{-\left(x-\mu_x^{(i)}\right)^2-\left(y-\mu_y^{(i)}\right)^2}{2r_d^2} \exp \frac{-\left(z-\mu_z^{(i)}\right)^2}{2r_d^2}$$

where n_{acid} is the number of released acids in the resist layer, $\mu_{x,y,z}$ the position of the acid and r_d the diffusion radius. We strive to replace this model by a more sophisticated model in the future. The determination of the (in)solubility close to the substrate and vacuum interface deserves special attention. The problem is that an acid cannot diffuse beyond the interface. Instead, we assume that an acid is reflected. The contribution of an acid to the (in)solubility is determined by using mirror symmetry at the vacuum and substrate interface. It is achieved by substituting the following expression,

$$\exp \frac{-\left(z-\mu_z^{(i)}\right)^2}{2r_d^2} \longrightarrow \exp \frac{-\left(z-\mu_z^{(i)}\right)^2}{2r_d^2} + \exp \frac{-\left(z+\mu_z^{(i)}-2z_s\right)^2}{2r_d^2} + \exp \frac{-\left(z+\mu_z^{(i)}-2z_v\right)^2}{2r_d^2}$$

Downloaded From: http://proceedings.spiedigitallibrary.org/ on 03/13/2017 Terms of Use: http://spiedigitallibrary.org/ss/termsofuse.aspx

where z_s defines the position of the substrate interface and z_v defines the position of the vacuum interface. The determination of the (in)solubility at a particular position in the resist layer is shown in Fig. 1 schematically. A three dimensional image of the (in)solubility of the exposed resist

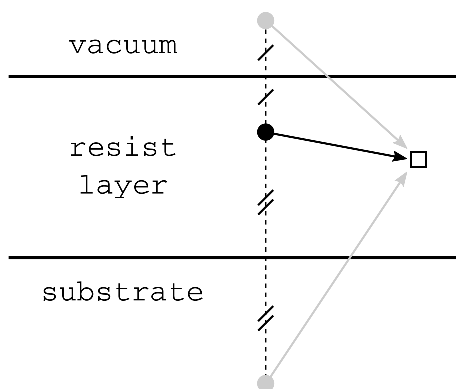

Figure 1: Schematic of the determination of the (in)solubility of a CAR at a particular location. The black sphere is the position of an acid in the resist layer, which is obtained with a Monte-Carlo electron-matter interaction simulator. Two mirrored acids (gray spheres) are virtually located in the substrate layer and in the vacuum. The mirrored acids are used for calculating the reflection of the acid diffusion with respect to the vacuum and substrate interface. The (in)solubility at the square marker is determined by evaluating a Gaussian kernel for the diffusion of the acid. The net (in)solubility at the square marker is obtained by accumulating the contributions of all released acids in the resist layer.

layer is then constructed by evaluating the expression $S(x, y, z)$ for each voxel. The computational complexity of the latter scales with the product of the dimensions of the three dimensional image and the number of acids in the resist layer. Typically, the computational complexity is $> 10^{12}$ and the computation time for the three dimensional image is reduced dramatically by using a graphics processing unit (GPU).

We now proceed similarly to the work of Refs. 4–6, where a threshold determines the boundary between exposed and unexposed resist. For a positive tone resist (PTR), intensities higher than the threshold in the three dimensional image are dissolvable in a developer. Analogously for a negative tone resist (NTR), intensities lower than the threshold are dissolvable. In reality, there is also a development phase, which we so far have ignored in this study. We acknowledge that this is a simplified view of post lithographic processing.

It is necessary, for realistic cases, that the elastic and inelastic scattering cross-sections of a CAR are available. The inelastic scattering cross-sections, for example, can be determined from optical loss functions, which can be obtained from optical experiments and from electron energy loss spectroscopy (EELS) measurements.[†] Unfortunately, we do not have the optical loss function of any particular CAR at our disposal. Therefore, we can only demonstrate the framework for the investigation of shotnoise induced SWR formation by using artificial scattering cross-sections. In our simulation tool, for example, we do have the scattering cross-sections for the organic resist PMMA. For the sake of demonstration, we will assume in the upcoming example that PMMA behaves as a CAR. We acknowledge that this is not a realistic approximation.

[†]More details on the sources for the scattering cross-sections, which are used in our Monte-Carlo electron-matter interaction simulator, can be found in Ref. 9.

Downloaded From: http://proceedings.spiedigitallibrary.org/ on 03/13/2017 Terms of Use: http://spiedigitallibrary.org/ss/termsofuse.aspx

3. EXAMPLE WITH ANALYSIS

Let us now give an example of the SWR formation. We define a 100 nm thick layer of PMMA on top of an infinitely thick silicon substrate and use the simulator of Ref. 9 for the purpose of lithography. We assume that the resist behaves as a NTR and write the pattern of an isolated line into the resist layer by scanning a beam with 20 keV electrons over an area of 32 nm×1 µm (width and length). During the exposure, we use a Gaussian spot size with FWHM=FW50%=20 nm, beam step size of 4 nm and a Poisson distributed exposure dose of 80 µC/cm^2, 60 µC/cm^2 and 40 µC/cm^2. During the exposure of the sample, we determine the distribution of released acids by recording the locations of the inelastic events within the resist layer. We now construct a three dimensional image of the (in)solubility of the resist layer within a cuboid of 128 nm(256px) wide, 800 nm(1024px) in length and 100 nm(128px) in height. The latter is obtained by evaluating expression $S(x, y, z)$ for each voxel in the three dimensional image, where we have used a three dimensional Gaussian with $\sigma_{x,y,z} = r_d$ =5 nm for the diffusion of the acid. Furthermore, we have normalized the three dimensional image such that the minimum value for the (in)solubility is zero and the maximum value is one. We are now ready to analyze the resulting image of the (in)solubility in different ways. Let us first look at the average (in)solubility in a xz-slice of the three dimensional image. The result of that is shown in Fig. 2, where we have marked the boundary between exposed and unexposed resist by contour lines for different values of the threshold. Notice the result of the scattering, which causes the distribution of the acids to broaden at increasing depth. In the remainder of the article, we arbitrarily choose a threshold of 0.5 with respect to the normalized (in)solubility to mark the boundary between exposed and unexposed resist. A yz-slice of the three dimensional

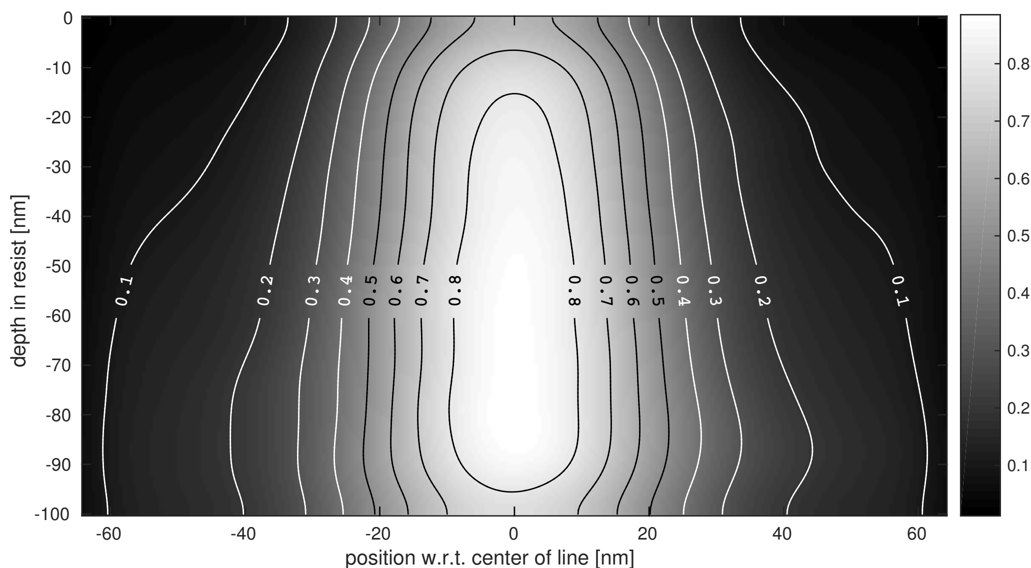

Figure 2: The average (in)solubility in a xz-slice of the three dimensional image. The sample consists of a 100 nm thick layer of CAR on top of an infinitely thick silicon substrate. A pattern of an isolated line is written into the resist layer by scanning a beam with 20 keV electrons over an area of 32 nm×1 µm (width and length) by using a Monte-Carlo electron-matter interaction simulator. The (in)solubility is obtained by accumulating the contributions of all acids in the resist layer, where we have used a three dimensional Gaussian with $\sigma_{x,y,z} = r_d$ =5 nm for the diffusion of the acid. The (in)solubility is normalized such that the minimum value for the (in)solubility is zero and the maximum value is one. The boundary between exposed and unexposed resist is shown by contour lines for different values of the threshold.

Downloaded From: http://proceedings.spiedigitallibrary.org/ on 03/13/2017 Terms of Use: http://spiedigitallibrary.org/ss/termsofuse.aspx

image, taken at a depth of 50 nm from the top surface of the resist layer, is shown in Fig. 3 for three different exposure doses. Notice that the boundary appears to have increasing roughness for decreasing dose (from left to right). We will discuss this effect in detail later on. Instead of a slice at a particular depth, we also construct a three dimensional view of the boundary between exposed and unexposed resist. The result for the left side of the boundary is shown in Fig. 4 for the three different exposure doses. Next, we determine the average LER as a function of the depth in the resist layer from the yz-slices by calculating the standard deviation (one-sigma) of the left and right boundary. If we repeat that procedure for all slices, ranging from the top of the resist layer to the bottom of the substrate, we obtain the result of Fig. 5: the average LER as a function of the depth in the resist layer. The observed increase in roughness for decreasing dose in Fig. 3 is confirmed by this calculation. This was also concluded in the work of Refs. 4–6 for two dimensional cases. In the current study, we observe the very same effect in a more sophisticated three dimensional model. In addition, we observe an interesting effect close to the vacuum and substrate interface: the roughness is increasing as we approach the interface.

Let us discuss the observed trends for shotnoise effects in SWR formation. Shotnoise effects arise due to the nature of Poisson statistics: the number of acids varies with the square root of the number of acids, i.e. $n_{\text{acid}} \pm \sqrt{n_{\text{acid}}}$. The ratio between the fluctuations and the number of acids is given by $\sqrt{n_{\text{acid}}}/n_{\text{acid}} = 1/\sqrt{n_{\text{acid}}}$. What this really means is that if we decrease the dose, and hence reduce the number of released acids, we get worse statistics. The result of that, as shown in Fig. 5, is an increase in roughness for decreasing dose. There are two contributions for the increase of roughness near the vacuum and substrate interface. One contribution relates to the actual number of acids, which is less near the interface than away from the interface. The explanation for this effect is as follows. Secondary electrons at the top of the resist layer escape into vacuum, and hence cannot contribute any further to acid release within the resist layer. At the bottom we have a similar effect: secondary electrons scatter into the silicon substrate. The difference is (with respect to the vacuum side) that secondary electrons are created in the silicon substrate. There are, however, fewer secondary electrons scattering from the silicon substrate back into the resist layer. Another contribution stems from the fact that no acids are found on the vacuum side nor on the substrate side. We will demonstrate the consequence on the statistics by example. Suppose that the distribution of acids in the resist layer is homogeneous and isotropic, i.e. the probability to find an acid anywhere in the resist layer is independent of position. The (in)solubility in the center of the resist layer is primarily determined by the contribution of $n \pm \sqrt{n}$ acids surrounding that position. There are no acids found beyond the interface and so near the interface we only have $\frac{1}{2}n \pm \sqrt{\frac{1}{2}n}$ acids in the resist layer to account for the (in)solubility. Remember that the acids in the resist layer are reflected by using mirror symmetry and hence we effectively have $n \pm \sqrt{2}\sqrt{n}$ (mirrored) acids contributing to the (in)solubility. We conclude that the statistics near an interface are worse because (1) the number of acids near the interface is less than away from the interface and (2) because there are no acids found beyond the interface.

Downloaded From: http://proceedings.spiedigitallibrary.org/ on 03/13/2017 Terms of Use: http://spiedigitallibrary.org/ss/termsofuse.aspx

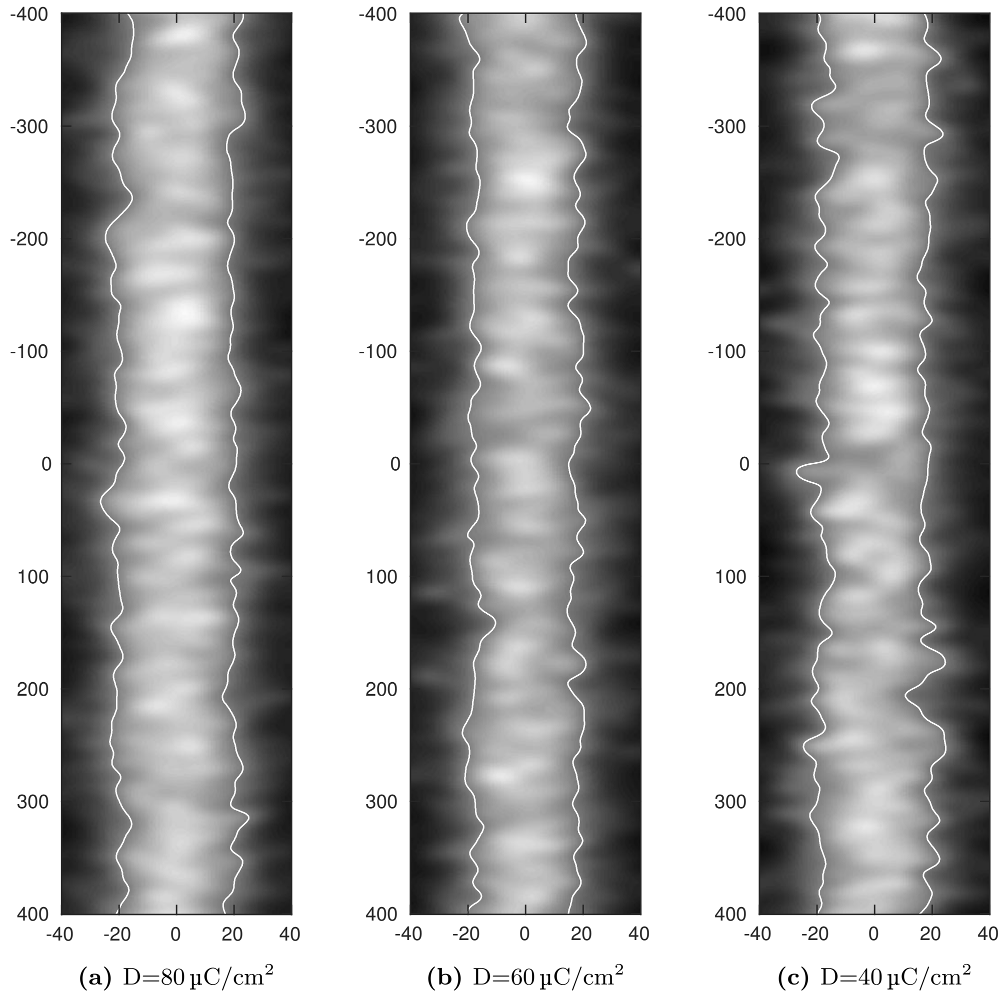

(a) D=80 µC/cm^2 **(b)** D=60 µC/cm^2 **(c)** D=40 µC/cm^2

Figure 3: A yz-slice of the simulated three dimensional (in)solubility of an exposed resist layer. The slice is taken at a depth of 50 nm from the top surface of a 100 nm thick layer of CAR, which is located on a infinitely thick silicon substrate. The white wavy lines mark the boundary between exposed and unexposed resist for a threshold of 0.5. The three subfigures (a)-(c) correspond to a Poisson distributed exposure dose of respectively 80 µC/cm^2, 60 µC/cm^2 and 40 µC/cm^2.

Downloaded From: http://proceedings.spiedigitallibrary.org/ on 03/13/2017 Terms of Use: http://spiedigitallibrary.org/ss/termsofuse.aspx

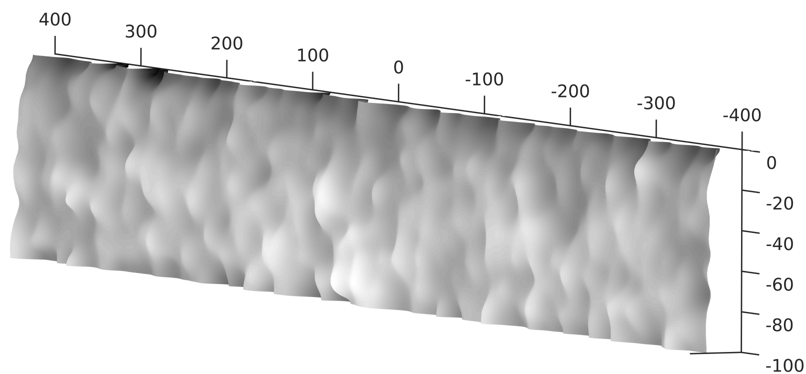

(a) D=80 µC/cm^2

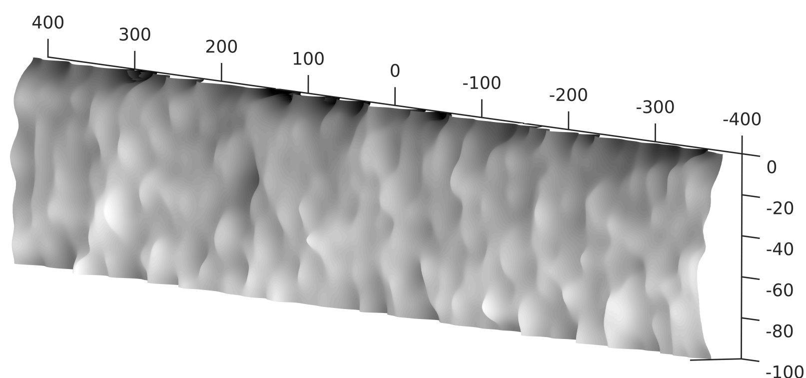

(b) D=60 µC/cm^2

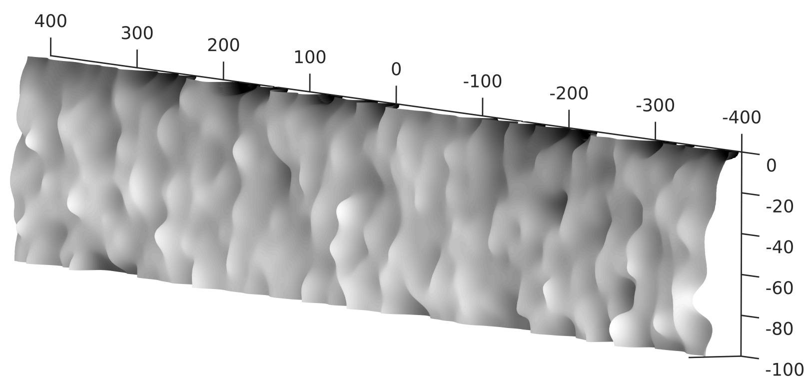

(c) D=40 µC/cm^2

Figure 4: A three dimensional view of the boundary between exposed and unexposed resist. The surfaces are obtained from a simulated exposure of a 100 nm thick layer of CAR, which is located on a infinitely thick silicon substrate. Similar to Fig. 3, the boundary between exposed and unexposed resist is determined with threshold of 0.5. The three subfigures (a)-(c) correspond to a Poisson distributed exposure dose of respectively 80 µC/cm^2, 60 µC/cm^2 and 40 µC/cm^2.

Downloaded From: http://proceedings.spiedigitallibrary.org/ on 03/13/2017 Terms of Use: http://spiedigitallibrary.org/ss/termsofuse.aspx

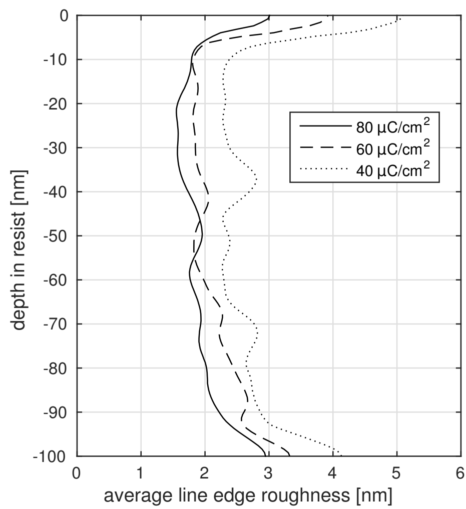

Figure 5: The average LER as a function of the depth. The figure is derived from yz-slices of the three dimensional image of the (in)solubility. The boundary between exposed and unexposed resist is determined with a threshold of 0.5. The average LER is obtained by calculating the standard deviation (one-sigma) of the left and right boundary. By considering all slices, ranging from the top of the resist layer to the bottom of the substrate, the average LER as a function of the depth from the top surface of the resist layer is obtained.

Downloaded From: http://proceedings.spiedigitallibrary.org/ on 03/13/2017 Terms of Use: http://spiedigitallibrary.org/ss/termsofuse.aspx

4. CONCLUSION

We have succeeded in creating a fast three dimensional Monte-Carlo framework for the investigation of shotnoise induced SWR formation. In comparison with existing studies, we simulate the electron-resist interaction by using an advanced Monte-Carlo program. We have considered a simplified model for the release of an acid from a PAG and used three dimensional Gaussian diffusion for the acids. The latter includes reflection of acids at the vacuum and substrate interface by using mirror symmetry. We can already see interesting effects such as: surface effects, broadening of the acid distribution in the resist layer due to the scattering and roughness as a function of the penetration depth.

This work is supported by NanoNextNL, a micro and nanotechnology program of the Dutch Government and 130 partners.

References

[1] Steenwinckel, D., Lammers, J. H., Leunissen, L. H. A. and Kwinten, J. A. J. M., "Lithographic importance of acid diffusion in chemically amplified resists", *Proceedings of SPIE* **5753**, 269–280 (2005).

[2] Gallatin, G. M., "Continuum model of shot noise and line edge roughness", *Proceedings of SPIE* **4404**, 123–132 (2001).

[3] Yuan, L. and Neureuther, A., "Investigation of shot-noise-induced line-edge roughness by continuous-model-based simulation", *Proceedings of SPIE* **5376**, 312–321 (2004).

[4] Kruit, P., Steenbrink, S. W. H. K, Jager, R. and Wieland, M., "Optimum dose for shot noise limited CD uniformity in electron-beam lithography", *Journal of Vacuum Science & Technology B: Microelectronics and Nanometer Structures* **22**, 2948 (2004).

[5] Kruit, P. and Steenbrink, S. W. H. K., "Local critical dimension variation from shot-noise related line edge roughness", *Journal of Vacuum Science & Technology B: Microelectronics and Nanometer Structures* **23**, 3033 (2005).

[6] Kruit, P. and Steenbrink, S. W. H. K., "Shot noise in electron-beam lithography and line-width measurements", *Scanning* **28**, 20–26 (2006).

[7] Neureuther, A. R., Pease, R. F. W., Yuan, L., Baghbani Parizi, K., Esfandyarpour, H., Poppe, W. J., Liddle, J. A. and Anderson, E. H., "Shot noise models for sequential processes and the role of lateral mixing", *Journal of Vacuum Science & Technology B: Microelectronics and Nanometer Structures* **24**, 1902 (2006).

[8] Patsis, G. P., Tsikrikas, N., Drygiannakis, D. and Raptis, I. "Detailed resist film modeling in stochastic lithography simulation for line-edge roughness quantification", *Microelectronic Engineering* **87**, 989–992 (2010).

[9] Verduin, T., Kruit, P., and Hagen, C. W., "The effect of sidewall roughness on line edge roughness in top-down scanning electron microscopy images", *Proceedings of SPIE* **9424**, 942405 (2015).

[10] Verduin, T., Kruit, P., and Hagen, C. W., "Determination of line edge roughness in low dose top-down scanning electron microscopy images", *Journal of Micro/Nanolithography, MEMS, and MOEMS* **13**, 033009 (2014).

Downloaded From: http://proceedings.spiedigitallibrary.org/ on 03/13/2017 Terms of Use: http://spiedigitallibrary.org/ss/termsofuse.aspx